International Journal of Innovative
Computing, Information and Control
Volume 8, Number 1(B), January 2012
 ISSN 1349-4198
pp. 953–965

A GENERIC INTELLIGENT OIL-GAS FLOW CLASSIFIER BASED ON ECT SENSOR DATA

Khursiah Zainal-Mokhtar and Junita Mohamad-Saleh*

School of Electrical and Electronic Engineering
Engineering Campus, Universiti Sains Malaysia
14300 Nibong Tebal, Penang, Malaysia
venconmigo1010@gmail.com; *Corresponding author: jms@eng.usm.my

Received October 2010; revised February 2011

Abstract. *Many flow regime classification systems based on Electrical Capacitance Tomography (ECT) sensor data have been developed, but they only focused on fixed ECT sensor parameters. Due to fixed sensor parameters, the systems are not generic because they can only work with data based on the particular ECT sensor parameters. This paper presents the work on developing a generic flow classifier which can flexibly accept data obtained from different ECT sensor parameter values. The generic system employs an Artificial Neural Network (ANN) trained with ECT data based on a range of ECT parameters. The developed system has shown to be able to handle ECT data of different sensor parameters and correctly classify their corresponding flow regimes to a certain degree of accuracy. Industries are able to save design costs by using such a system.*
Keywords: Generic classifier, Flow regime, Electrical capacitance tomography, Artificial neural network

1. **Introduction.** Multiphase flows have been employed frequently in numerous industrial applications such as petroleum extraction and processing, nuclear power plant and various chemical reactors. Therefore, an understanding of the internal characteristics of such processes is critical. The information on dynamic flows is certainly one of the most important subjects to enact the efficiency and safety in aggressively fast-moving fluids of multiphase mixture in a process equipment. This justifies the large number of technical and scientific studies in this area, some of which have focused on specific applications such as modelling of pressure drop [1,2] and heat transfer correlations [3,4] and others on wider aspects such as the construction of systems that used various methods for identification of multiphase flow regime.

In 1970s, researchers in the petroleum industry began to predict flow regimes in liquid columns using some basic physical mechanisms which have been used in other industries. During this time, Wallis and Dobson [5] published a simple criterion to predict flow regime transition based on the relations of geometrical parameters of a pipe and liquid velocity. Hubbard and Dukler [6] suggested a method by which the flow pattern can be determined from the spectral distribution of the wall pressure dustribution. Other researches by Govier et al. [7], Chaudry et al. [8] and Isbin et al. [9] have tried to relate the flow pattern to the pressure gradient variation. While all these studies have contributed to the understanding of flow regime classification, the traditional identification methods of flow regime have some shortcomings such as high requirements of complex measuring systems and production of non-systematic results. Besides, there is also a conventional way to classify flow regimes based on visual observation using high speed photography and video. The major difficulty in visual observation is that the pictures produced are often confusing and difficult to interpret, especially when dealing with high velocity flows.

Moreover, visual observation can only be successful in transparent process equipments, and thus flow visualisation is impossible in opaque systems. Hence, an alternative to the traditional classification methods and a conventional way of classifying flow regime is required.

Various modalities of process tomography have been developed for flow observation and measurement in the past few decades [10]. X-ray, the earliest tomography system, has not only been used in the medical field but also in industry. For instance, work by Jones and Zuber [11] obtained the probability density function of void fraction measured by an x-ray absorption technique. Even though x-ray tomography can be applied non-invasively through metal containers, the potential hazards of using radioactive and ionizing radiation, along with high costs for installation and operation, remain as major concerns. Examples on other tomographic techniques for visualisation and flow regime identification can be found in [12-18]. However, these techniques require bulky equipment, high installation cost, considerable maintenance and are dangerous. Therefore, it is highly attractive to have relatively simple and cheap tomography technique, which is capable of obtaining measurements non-invasively, non-intrusively and with no radiation involved.

Electrical Capacitance Tomography (ECT) is a measuring technique suitable for industrial processes involving non-conducting mixture such as gas-oil [19-21]. In ECT, several electrodes are mounted around a process equipment. These electrodes measure the changes in the capacitance between all possible pairs of electrodes for various material distribution. From these measurements of capacitance changes, a cross-sectional image can be reconstructed with the aid of an image reconstruction algorithm. In turn, process flow parameters can be interpreted from the cross-sectional image based on further calculation and analysis.

The Linear Back Projection (LBP) algorithm [19] is the first and simplest reconstruction algorithm ever proposed for ECT [22]. However, images produced by LBP algorithm appear distorted due to the soft-field effect [23]. This fact has prompted many researchers to opt for different reconstruction methods to overcome the problem associated with the conventional image reconstruction algorithm. The work by Noralahiyan et al. [24] was the first to show the capability of ANN in reconstructing accurate tomography images. Besides an ANN approach, a number of improved or new algorithms have been introduced to obtain more accurate images. These include the Landweber [25-27] and Tikhonov algorithms [28-30]. Although the advanced reconstruction methods have shown to be able to produce slightly more accurate images for some flow regimes, distortion of images is still a problem for other regimes. Furthermore, the process of image reconstruction is time-consuming [31].

Many researchers have then devoted to the study on obtaining better accuracy of process interpretation in a much shorter processing time by employing a direct ANN method without going through the time-consuming image reconstruction phase. In research by Sun et al. [32], ECT data in a form of differential pressure signal are processed using wavelet analysis to extract six significant features. Then, a Multi-Layer Perceptron (MLP) neural network is adopted to train the features and classify four different flow regimes, namely annular, bubble, plug and slug flows. The correct flow regime identification percentage obtained was 86.76%. Yan et al. [33] presented 10 features extracted from ECT measurements to an MLP. Then, the MLP neural network which is utilised was trained with the features to classify eight different flow regimes. The MLP attained an average of 93.7% correct identification percentage. Barbosa et al. [34] considered two different types of two-phase flows; gas-solid and gas-liquid, in flow regime identification using a Self Organizing Map (SOM) neural network. The data used contain not only ECT

measurements but also values of pressure drop and fluctuating pressure in a pipe. Using this data, the ANN is trained to identify four different flow regimes and obtain 66.67% of overall identification percentage. Meanwile, Yu et al. [35] used the Principle Component Analysis (PCA) method to reduce 66 ECT values to only 10 principle components. An MLP network was trained and the results showed the ability of MLP to correctly classify six different flow regimes for over 96% recognition rate.

Despite the successes of previous works for flow regime classification based on ANN approach, they all focused on fixed ECT sensor parameters, producing interpretation systems that were not generic. The employed ANNs were trained based on fixed ECT sensor parameters making them limited in "intelligence" and hence they cannot give accurate process interpretation and for data of different sensor parameter values [36]. Therefore, it would be desirable to have an intelligent system which can accommodate a range of sensor parameter values. Such a system would be an intelligent generic flow regime classifier that is able to save cost.

2. **ECT System.** Figure 1 illustrates the basic components of an ECT system; the sensors, data acquisition system (DAS) and a computer system. The primary sensor consists of copper electrode plates mounted equidistantly around the periphery of an insulating process equipment. Different materials have different values of dielectric constants also known as relative permittivities. Hence, the distribution of two-component flows within an ECT sensing region produces a change in the capacitance measurements between two electrodes. This fundamental theory is used in ECT. Experiments have found that the sensitivity of an ECT sensor greatly depends on the electrode angular angle whilst other ECT sensor parameters can be considered insignificant [37].

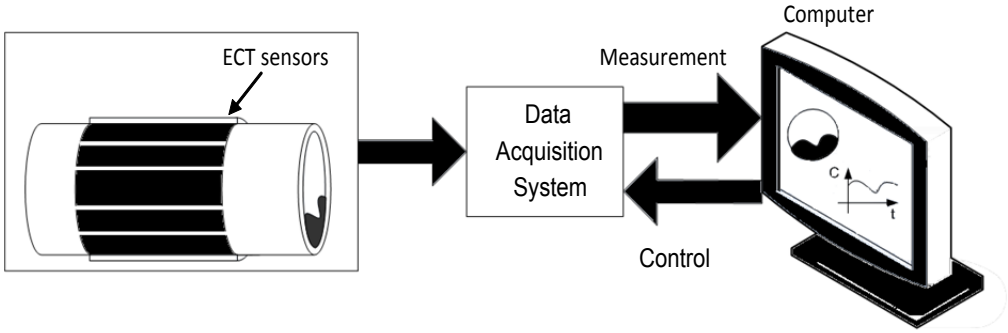

FIGURE 1. A schematic diagram of an ECT system

The sensors measure the capacitances of all possible electrode combinations. These measurements are taken by the DAS which is also responsible for converting the ECT measurements into digital signal and sending the signal to the computer system. The computer has two main functions. First, it controls the measurement operations performed by the capacitance sensors. Second, by means of an appropriate algorithm, it uses the measured capacitance data to produce useful information represented either qualitatively in the form of a reconstructed image of flow process or quantitatively in the form of flow parameter estimations.

The current work aims to develop a generic intelligent system for classification of gas-oil flow regimes from ECT data. As previous literature work has shown that the primary electrode size is the most significant sensor parameter, this work specifically focuses on using a range of ECT primary electrode sizes to produce a generic intelligent flow regime classifier.

3. **Approach and Method.** Figure 2 illustrates the ECT sensor parameters used in this investigation. As reported by Flores et al. in 2005 [38], the sensors with driven guards possess large effective sensing space with a condition that the size of electrode must be as large as possible. This finding shows that the size of electrode plays an important role in determining the effectiveness of sensor sensitivity. Hence, this investigation focuses on varying the sensor electrode size.

3.1. **12-electrode ECT sensor design.** The number of electrodes used is 12 to compensate for the tradeoff between sensitivity (i.e., low if too many electrodes such as 16 is used) and resolution (i.e., low if less number of electrodes such as 8 is used) [38]. As shown in Figure 2 the inner pipe (R1), outer pipe (R2) and screen (R3) walls have been chosen to be 1, 1.05 and 1.15 units, respectively. The guard electrodes α have subtended angle of 2° while the primary electrode sizes, θ are varied.

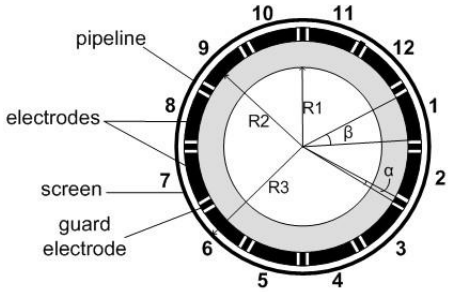

FIGURE 2. ECT sensor model

For a 12-electrode ECT system, it is possible to obtain 66 capacitance values from pairs of electrodes based on [39]

$$N = \frac{n(n-1)}{2} \tag{1}$$

where N is the total number of capacitance measurements and n is the number of electrodes.

In ECT, high sensor sensitivity is important, hence the primary electrode size, θ are chosen to vary within $[20°, 26°]$ with 0.5° intervals. The minimum size of 20° and no smaller is chosen because too small a primary electrode angle leads to lower sensitivity of the ECT sensor [20]. The maximum size of θ is selected to be 26°. Larger than 26° results in ECT sensors without guard electrodes due to insufficient spacing.

Figure 3 shows the schematic diagrams of six commonly formed flow regimes. These flows are used in the training process to develop the generic intelligent classifier system.

3.2. **ECT dataset collection.** There are two types of ECT data; the actual plant data and the ECT simulated data. In this work, the simulated ECT data [40] are used to facilitate the generation, regeneration and repetition of various complex flow patterns that are required for the purpose of training an intelligent system. The numbers of flow patterns simulated for each flow regime are given in Table 1. Only one empty and full flow patterns can be generated for each θ. Unlike the full and empty flows, many stratified flows can be simulated based on different oil heights as well as different tilted angles of gas-oil interface. Similarly, bubble flow patterns can be simulated based on various bubble radii as well as different bubble locations and thus, a large number of this flow regime can

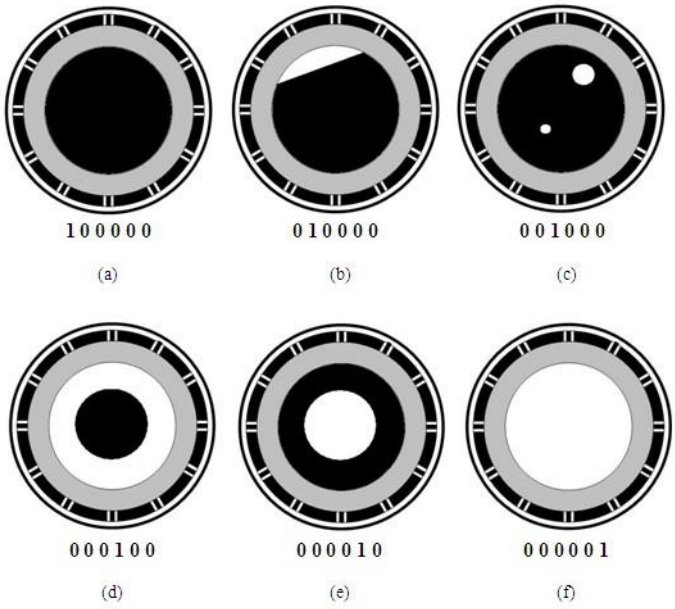

FIGURE 3. A schematic diagram of the flow regimes to be classified with their corresponding class representation (a) empty (b) full (c) bubble (d) stratified (e) annular (f) core

TABLE 1. Number of flow patterns used for each flow regime of a single θ

Flow Regime	Number of data
Full	1
Stratified	1224
Bubble	1436
Core	199
Annular	199
Empty	1

be generated. The annular and core flows are just the opposite of each other and their flow patterns are simulated by varying the sizes of air or oil core, respectively.

3.3. **Development of generic intelligent classification system.** In this work, the intelligent system is based on an ANN. An ANN can be classified by the type of learning scheme; either supervised or unsupervised. Each learning scheme can be categorised into its architectural types. Unsupervised learning is not as good as supervised learning at classification task [41]. Hence, only supervised learning is considered in this work. There are three types of supervised ANN architectures; Single-Layer Feed-Forward (SLFF), Multi-Layer Feed-Forward (MLFF) and recurrent. To develop an intelligent system, a variant of the supervised MLFF ANN known as the Multi-Layer Perceptron (MLP) is selected due to its simple structure, but yet capable of solving most nonlinear problems. Classification is one of the most successful applications that has been solved with MLP. The MLPs are programmed to learn various input patterns in association to corresponding classes or categories. After learning, it has to correctly classify any unseen set of patterns into one of the possible classes. Furthermore, its simple structure results in high execution speed compared with other ANN models. Hence, it is employed in this work.

Figure 4 shows the architecture of an MLFF ANN. An MLP consists of three layers; an input layer, an intermediate hidden layer and an output layer. Input signals, x_1, x_2, ..., x_n are fed to an MLP via its input neurons. Then, these input neurons pass the signals to the hidden neurons via the input weight connections, w_{11}, w_{21}, ..., w_{4n}. The hidden neurons execute some computations and transmit the results to the output neurons via the output weight connections, $w2_{11}$, $w2_{21}$, ..., $w2_{m4}$. The output neurons then carry out further computation and present the final results, y_1, ..., y_m.

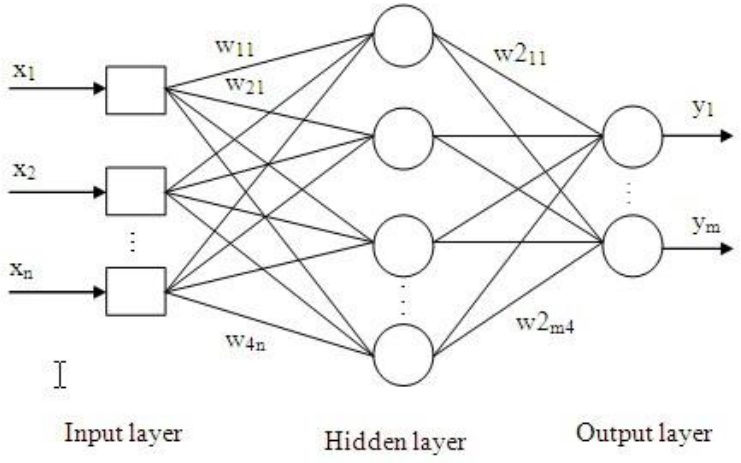

FIGURE 4. A schematic diagram of multi-layer perceptron (MLP) for neural network [41]

A three-layer MLP networks with 66 input neurons (for 66 capacitance measurements) and 6 output neurons (six flow regimes as shown in Figure 3 has been designed for this investigation. The number of optimal hidden neurons is determined experimentally.

Each output neuron should give the value of either '0' or '1'; therefore, the most suitable transfer function to be applied to each of them is the logarithmic sigmoid (log). As for the hidden neurons, hyberbolic tangent (tanh) sigmoid transfer function is applied because the input values of the hidden neurons are within $[-\infty, +\infty]$. Hence, a tanh function provides a larger range of transfer. The Levenberg-Marquardt (LM) training algorithm is used because it is one of the best and most commonly used algorithm for classification applications [42,43]. It also has the ability to avoid local minima trap, a problem that often occurs in ANN training [44].

Besides local minima trap, over-training is another problem in ANN learning. Over-training can lead to over-fitting of training data which leads an MLP to memorise the training data and become inflexible and hence, incapable of generalising. This situation degrades the MLP's performance over new sets of data. To avoid the MLP from being overtrained, cross-validation method is used [45]. This is a well-established early stopping method when a separate data set known as the validation set is incorported into the training process to check for the ANN's generalisation performance. Based on validation method, a training process is terminated when there is no longer improvement in the validation performance. This way the ANN is not overtrained.

In this study, raw simulated data has been used to train the MLP toward developing a generic classification system. Raw data are used because the system needs to be generic and able to deal with a vast range of ECT θ parameter. Various experimental methods have been devised for investigation towards developing generic classifier as illustrated in Figure 5. They are:

(a) Method A is a common method used by all previous researchers whereby the MLP is trained with ECT data involving flow patterns generated with one θ. This is a non-generic method aimed as comparison purpose. 1250 simulated data are generated for each θ and divided into training, validation and testing sets with 4:2:4 ration, respectively. In this investigation, separate MLPs are trained with ECT data of a single θ in the range $[20°, 26°]$ with $1°$ interval. The MLPs are then tested with unseen ECT data.

(b) Method B is employed by training separate MLPs with ECT data of a single θ. The MLPs are tested with data of other θs. This method is used to test the generic capability of the intelligent system other than trained θ values.

(c) Method C involves training an MLP based on ECT data that contain various flow regimes of various θ ranging from $20°$ to $26°$ with $1°$ interval. 2750 simulated data are used for the training process. Then, the MLP is tested with unseen data of $\theta = [20°, 26°]$.

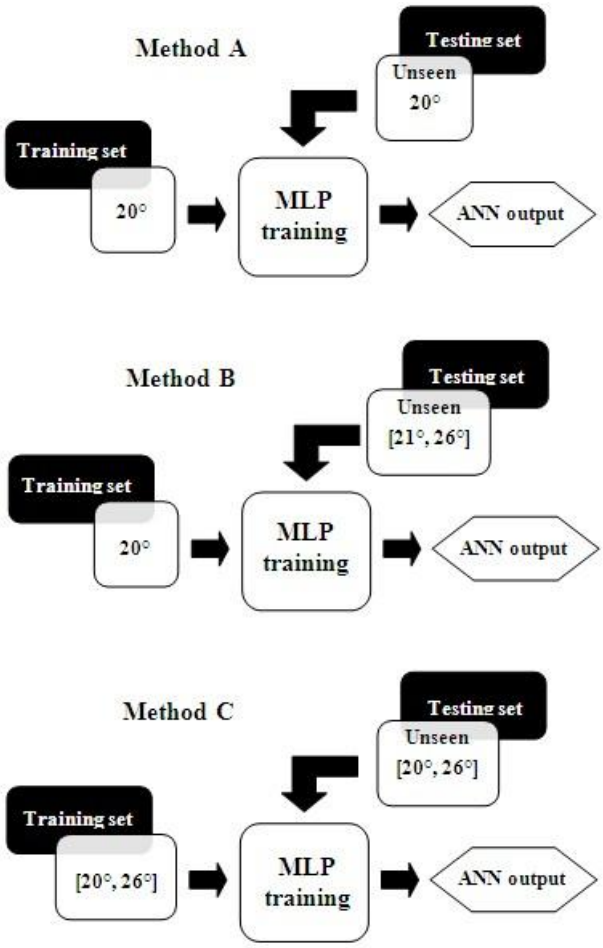

FIGURE 5. Schematic diagram of proposed methods A, B and C

Upon completion of the MLP training processes for all methods, the best network of each method is chosen based on the testing data set. The performance of the MLP is evaluated based on the highest correct classification percentage (CCP) given by,

$$Best\,performed\,MLP = Max\left[\left(\frac{Number\,of\,correctly\,classified\,data}{Total\,number\,of\,data}\right)\times 100\%\right] \quad (2)$$

The best MLP is then executed with a total of 6000 verification data. The verification data are ECT data obtained from θ values other than the sizes used during the training

process. They are θ values of 20.5°, 21.5°, 22.5°, 23.5°, 24.5° and 25.5°. The MLP training process is illustrated in Figure 6.

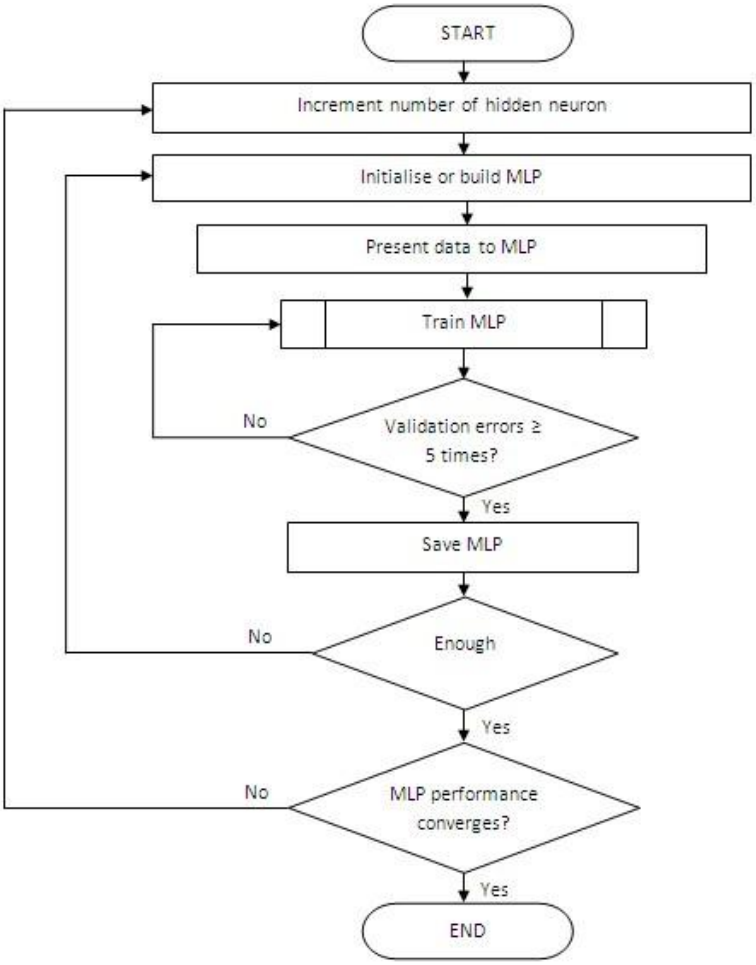

FIGURE 6. Flowchart of MLP training process

4. **Results and Discussion.** The MLP training results for Models A is depicted in Table 2. From Table 2, it can be seen that a MLP with θ of 23° achieved the highest CCP which is 90.2% followed closely by a MLP with θ of 26° with CCP of 90%. However, the MLP trained with $\theta = 23°$ failed to classify full flow regime whereas an MLP trained with $\theta = 26°$ has been able to classify full flow with CCP of 100% while other MLPs have failed. This means that other MLPs are unable to classify full flow when trained with only 50 data sets of this flow regime. Hence, in order to increase the capability of the MLPs in classifying the full flow, the data of this flow regime may need to be repeated more than 50 times. By looking at the competency of each MLP at classifying all flow regimes, the MLP with $\theta = 26°$ is the best network as it is able to successfully obtained high CCP for all flow regimes. This is explained by its largest θ value, leading towards highest sensitivity within the sensing region.

Table 3 shows the results for Method B. It can be seen that the overall performances deteriorate for all flow regimes. This means all the MLPs cannot generalise the new data sets which are totally distinct from its training set. For example, an MLP that has been trained with ECT data of $\theta = 20°$ is not be able to respond correctly when presented with

Table 2. CCP for method A

Flow	Correct classification percentage (%)						
	20°	21°	22°	23°	24°	25°	26°
Full	0.00	0.00	0.00	0.00	0.00	0.00	100.00
Stratified	80.00	84.00	77.00	89.00	80.50	79.50	85.00
Bubble	91.00	93.00	93.50	92.50	92.50	88.50	93.00
Annular	95.92	79.59	91.84	97.96	83.67	77.55	91.84
Core	100.00	93.88	85.71	79.59	100.00	95.92	95.92
Empty	100.00	100.00	100.00	100.00	100.00	100.00	100.00
Overall CCP	87.80	88.00	85.80	90.20	87.40	84.40	90.00

Table 3. CCP for model B

Flow	Correct classification percentage (%)						
	20°	21°	22°	23°	24°	25°	26°
Full	0.0	0.0	0.0	0.0	0.0	0.0	0.0
Stratified	58.0	22.0	56.0	66.0	80.0	60.0	83.0
Bubble	63.0	84.0	67.0	3.0	34.0	17.0	0
Annular	64.0	63.0	28.0	66.0	32.0	19.0	7.0
Core	23.0	49.0	44.0	69.0	43.0	81.0	99.0
Empty	0.0	0.0	0.0	16.0	0.0	82.0	0.0
Overall CCP	41.6	43.6	39	42.4	37.8	43.6	37.8

Table 4. CCP for model C

Flow	CCP(%)
Full	100.00
Stratified	75.00
Bubble	71.00
Annular	86.00
Core	96.00
Empty	100.00
Overall CCP	93.46

data based on $\theta = [21°, 22°, \ldots, 26°]$ because the dissimilarity of patterns between the training and testing sets. This demonstrates poor classification ability of MLP developed based on Method B. Hence, this Method B is not able to produce a generic classifier.

Table 4 shows the CCP values achieved for Method C. The overall peformance is 93.46%, which is the highest of the three methods. Empty and full flows achieved 100% CCP each as a result of repeated data. Core flow attained CCP of 96% followed by annular 86%, stratified 75% and bubble 71%. Therefore, Method C has been proved successful and can be employed in developing an intelligent generic classifier system.

To further verify the generalisation performance of the best trained MLPs from the three methods, they have been tested with ECT data based on flow regimes from $\theta =$ 20.5°, 21.5°, 22.5°, 23.5°, 24.5° and 25.5° which are different from the training and testing sets. Each of the θ consisted of 1000 verification ECT data from various flow patterns.

Table 5. CCP (%) of the best MLP from method A

Flow Regime	20.5°	21.5°	22.5°	23.5°	24.5°	25.5°
Full	0.00	0.00	0.00	0.00	0.00	0.00
Stratified	0.00	0.00	2.33	7.67	26.67	50.67
Bubble	0.00	0.00	0.00	0.00	0.00	0.00
Core	0.00	0.00	0.00	1.51	4.02	17.09
Annular	0.00	0.00	0.00	0.00	4.02	17.59
Empty	0.00	0.00	0.00	0.00	0.00	0.00
Overall CCP	0.00	0.00	0.70	2.60	9.60	22.10

Table 6. CCP (%) of the best MLP from method B

Flow Regime	20.5°	21.5°	22.5°	23.5°	24.5°	25.5°
Full	0.00	0.00	0.00	0.00	0.00	0.00
Stratified	55.67	60.33	63.00	66.33	73.33	51.33
Bubble	0.00	0.00	0.00	0.00	6.67	72.67
Core	83.42	86.43	46.23	93.47	95.48	83.92
Annular	0.00	0.00	6.53	30.15	63.32	79.40
Empty	100.00	100.00	100.00	100.00	0.00	0.00
Overall CCP	33.40	35.40	29.50	44.60	55.60	69.70

Table 7. CCP (%) of the best MLP from method C

Flow Regime	20.5°	21.5°	22.5°	23.5°	24.5°	25.5°
Full	0.00	100.00	0.00	0.00	0.00	0.00
Stratified	67.00	70.33	69.97	72.67	73.67	74.33
Bubble	52.67	84.67	28.67	88.67	93.00	85.00
Core	92.96	92.46	48.24	92.46	98.49	93.47
Annular	85.93	51.76.91	88.94	83.42	69.85	82.91
Empty	100	100	100	100	100	100
Overall CCP	71.60	75.40	59.60	83.50	83.60	84.30

Tables 5 and 6 show the overall performance for the best MLPs from Methods A and B, respectively. The best MLP from Method A has shown its incapability at classifying flow regimes generated from different θ. Meanwhile, the best MLP from Method B has achieved satisfactory classification for only two flow regimes which are stratified and core. The CCP results of the best MLP for Method C are depicted in Table 7 showing that the MLP network is able to correctly classify the ECT data based on θ which are different from the training set. The overall CCP for 20.5°, 21.5°, 22.5°, 23.5°, 24.5° and 25.5° are 71.6%, 75.4%, 56.9%, 83.5%, 83.6% and 84.3%, respectively. The results demonstrate that a generic flow classifier can be developed by training an MLP with ECT data of various θ involving various flow patterns.

5. **Conclusion.** A generic classifier is more desirable in industry in order to save design cost. Previous works have only focused on developing classifier based on fixed ECT sensor parameters. This paper presented the development of a generic intelligent flow regime classifier based on ECT data. This investigation chose to include various ECT primary sensor electrode size in the quest of developing a generic flow regime classifier by employing MLP ANN. Three methods A, B and C of MLP training have been investigated for the purpose. The results from Method C show that it is feasible to develop a generic classifier for ECT data by training MLPs with ECT data based on different electrode sizes of various flow regimes.

In the future, it would be interesting to consider other ANN architectures such as the Hybrid-MLP for possibility of improving the performance of the generic classifier.

Acknowledgement. The authors wish to thank the Ministry of Science, Technology and Innovation (MOSTI), Malaysia for financially supporting this research under eScience fund grant No. 03-01-05-SF0134 and MOHE for the Fundamental research grant Scheme, No. 203/PELECT/6071148.

REFERENCES

[1] V. Singh and L. O. Simon, Predicting pressure drop in pneumatic conveying using discrete element modelling approach, *The 7th Conference on CFD in the Minerals and Process Industries (CSIRO)*, Melbourne, Australia, 2009.

[2] H. J. Lee, D. Y. Liu and Y. Alyousef, Generalized two-phase pressure drop and heat transfer correlations in evaporative micro/minichannels, *J. Heat Transfer*, vol.132, no.4, 2010.

[3] H.-Q. Zhang, Q. Wang, C. Sarica and J. P. Brill, Unified model of heat transfer in gas/liquid pipe flow, *SPE Prod & Oper*, vol.21, no.1, pp.114-122, 2006.

[4] Y. H. Wu and B. Wiwatanapataphee, Modelling of turbulent flow and multi-phase heat transfer under electromagnetic force, *Discrete and Continuous Dynamical System – Series B*, vol.8, no.3, pp.695-706, 2007.

[5] G. B. Wallis and J. E. Dodson, The onset of slugging in horizontal stratified air-water flow, *Int. J. Multiphase Flow*, vol.1, no.1, pp.173-193, 1973.

[6] M. G. Hubbard and A. E. Dukler, The characterization of flow regimes for horizontal two-phase flow, *Proc. of 1966 Heat Transfer and Fluid Mechanics Institute*, 1966.

[7] G. W. Govier, B. A. Radford and J. S. C. Dunn, The upward vertical flow of air water mixtures – Part 1: Effect of air and water rates on flow patterns, hold-up and pressure drop, *Can. J. Chem. Engng*, pp.58-70, 1957.

[8] A. B. Chaudhry, A. C. Emerton and R. Jackson, Flow regimes in the concurrent upwards flow of water and air, *The Symp. on Two-Phase Flow, Exeter*, pp.21-23, 1965.

[9] H. S. Isbin, R. H. Moen, R. O. Wickey, D. R. Mosher and H. C. Larson, Two-phase steam water pressure drop, *Chem. Engng Symp.*, vol.55, no.23, pp.75-84, 1959.

[10] M. S. Beck and R. A. Williams, Process tomography: A European innovation and its applications, *Meas. Sci. Technol.*, vol.7, pp.215-224, 1996.

[11] O. C. Jones and N. Zuber, The interrelation between void fraction flunctuations and flow patterns in two-phase flow, *Int. J. Multiphase Flow*, vol.2, pp.273-306, 1975.

[12] L. J. Xu and L. A. Xu, Gas/liquid two-phase flow regime identification by ultrasonic tomography, *Flow Meas. Instrum.*, vol.8, no.3-4, pp.145-155, 1997.

[13] M. H. Fazalul Rahimin, R. Abdul Rahim and J. Pusppanathan, Two-phase flow regime identification by ultrasonic computerized tomography, *Sensors and Transducers Journal*, vol.116, no.5, pp.76-82, 2010.

[14] R. Abdul Rahim, R. G. Green, N. Horbury, F. J. Dickin, B. D. Naylor and T. P. Pridmore, Further development of a tomographic imaging system using optical fibres for pneumatic convayers, *Meas. Sci. Technol.*, vol.7, pp.419-422, 1996.

[15] C. Yan, J. Zhong, Y. Liao, S. Lai, M. Zhang and D. Gao, Design of an applied optical fibre process tomography system, *Sensor and Actuators B: Chemical*, vol.104, no.2, pp.324-331, 2005.

[16] S. Z. Mohd Muji, R. Abdul Rahim and M. Morsin, Criteria for sensor selection in optical tomography, *IEEE Symposium on Industrial Electronics and Applications*, Kuala Lumpur, Malaysia, 2009.

[17] D. L. George, K. A. Shollenberger, J. R. Torczynski, T. J. O'Hern and S. L. Ceccio, Three-phase material distribution measurements in vertical flow using gamma-densitometry tomography and electrical-impedance tomography, *Int. J. Multiphase Flow*, vol.27, no.11, pp.1903-1930, 2001.

[18] U. Z. Ijaz, J.-H. Kim, A. K. Khambampati, M.-C. Kim, S. Kim and K.-Y. Kim, Concentration distribution estimation of fluid through electrical impedance tomography based on interacting multiple model scheme, *Flow Meas. Instrum.*, vol.18, no.1, pp.47-56, 2007.

[19] C. G. Xie, A. Plaskowski and M. S. Beck, 8-electrode capacitance system for two-component flow identification: Tomographic flow imaging, *IEE Proc.*, vol.136, no.4, pp.173-183, 1989.

[20] C. G. Xie, S. M. Huang, B. S. Hoyle, R. Thorn, C. Lenn, D. Snowden and M. S. Beck, Electrical capacitance tomography for flow imaging: System model for development of image reconstruction algorithms and design of primary sensors, *IEE Proc.-G*, vol.139, no.1, pp.89-98, 1992.

[21] W. Q. Yang, M. S. Beck and M. Byars, Electrical capacitance tomography: From design to applications, *Meas. Control*, vol.28, no.9, pp.261-266, 1995.

[22] H. K. Ji, Y. C. Bong and Y. K. Kyung, Novel iterative image reconstruction algorithm for electrical capacitance tomography: Directional algebraic technique, *IEICE T. Fund. Electr.*, vol.E89-A, no.6, pp.1578-1584, 2006.

[23] B. Su, Y. Zhang, L. Peng, D. Yao and B. Zhang, The use of simultaneous iterative reconstruction technique for electrical capacitance tomography, *Chem. Eng. J.*, vol.77, no.1-2, pp.37-41, 2000.

[24] A. Y. Nooralahiyan, B. S. Hoyle and N. J. Bailey, Pattern and association and feature extraction in electrical capacitance tomography, *Proc. of European Concerted Action on Process Tomography (ECAPT)*, Oporto, Portugal, 1994.

[25] W. Q. Yang, D. M. Spink, T. A. York and H. McCann, An image reconstruction algorithm based on Landweber's iteration for electrical-capacitance tomography, *Meas. Sci. Technol.*, vol.10, no.11, pp.1065-1069, 1999.

[26] G. Lu, L. Peng, B. Zhang and Y. Liao, Preconditioned Landweber iteration algorithm for electrical capacitance tomography, *Flow Meas. Instrum.*, vol.16, pp.163-167, 2005.

[27] Y. Li and W. Q. Yang, Image reconstruction by nonlinear Landweber iteration for complicated distribution, *Meas. Sci. Technol.*, vol.19, no.9, pp.1-8, 2008.

[28] S. H. Lee, S. B. Lee, Y. S. Kim, J. H. Kim, B. Y. Choi and K. Y. Kim, A filtering approach of iterative Tikhonov regularization method in ECT, *The 5th IEEE Conference on Sensors*, Daegu, Korea, 2006.

[29] L. Wang, X. Du and X. Shao, A hybrid ECT image reconstruction based in Tikhonov regularisation theory and SIRT algorithm, *J. Phys.: Conf. Ser.*, vol.48, pp.1453-1458, 2006.

[30] J. Lei, L. Shi, Z. Li and M. Sun, An image reconstruction algorithm based on the extended Tikhonov regularisation method for electrical capacitance tomography, *Measurement*, vol.42, pp.368-376, 2009.

[31] W. Wang, Voidage measurement of gas-oil two-phase flow, *Chin. J. Chem. Eng.*, vol.15, no.3, pp.339-344, 2007.

[32] T. Sun, H. G. Zhang and C. Y. Hu, Identification of gas-liquid two-phase flow regime and quality, *IEEE Instrumentation and Measurement Technology Conference*, Anchorage, AK, USA, 2002.

[33] H. Yan, Y. H. Liu and H. T Liu, Identification of flow regimes using back-propagation networks trained on simulated data based on a capacitance tomography sensor, *Meas. Sci. Technol.*, vol.15, no.2, pp.432-436, 2004.

[34] P. R. Barbosa, K. C. O. Grivelaro and P. Seleghim Jr., On the application of self-organizing neural networks on gas-liquid and gas-solid flow regime identification, *J. of the Braz. Soc. of Mech. Sci. & Eng.*, vol.12, no.1, pp.15-20, 2010.

[35] C. Yu, S. Yuchen and Z. Jian, A novel principle component analysis flow pattern identification algorithm for electrical capacitance tomography system, *2010 International Conference on Machine Vision and Human-Machine Interface*, 2010.

[36] J. Mohamad-Saleh and B. S. Hoyle, Determination of multi-component flow process parameters based on electrical capacitance tomography data using artificial neural networks, *Meas. Sci. Technol.*, vol.13, pp.1815-1821, 2002.

[37] A. M. Olmos, J. A. Primicia and J. L. F. Marron, Simulation design of electrical capacitance tomography sensors, *IET Sci. Meas. Technol.*, vol.1, no.4, pp.216-223, 2007.

[38] N. Flores, J. C. Gamio, C. Ortiz-Alemán and E. Damián, Sensor modeling for an electrical capacitance tomography system applied to oil industry, *Proc. of the COMSOL Multiphysics User's Conference*, Boston, USA, 2005.

[39] K. J. Alme and S. Mylvaganam, Electrical capacitance tomography – Sensor models, design, simulations, and experimental verification, *IEEE Sensors Journal*, vol.6, no.5, pp.1256-1266, 2006.

[40] D. M. Spink, Direct finite element solution for the capacitance, conductance or inductance, and force in linear electrostatic and magnetostatic problems, *The International Journal for Computation & Mathematics in Electrical & Electronic Engineering*, vol.15, no.3, pp.70-84, 1996.

[41] I. Saboori, M. B. Menhaj and B. Karimi, A non-linear adaptive observer based on neural networks for nonlinear systems including secure communication problems, *International Journal of Innovative Computing, Information and Control*, vol.6, no.11, pp.4771-4782, 2010.

[42] S. Basterrech, S. Mohammed, G. Rubino and M. Soliman, Lavenberg-marquardt training algorithms for random neural networks, *The Computer Journal*, vol.54, no.1, pp.125-135, 2009.

[43] A. Moghadassi, F. Parvizian and S. M. Hosseini, A new approach based on artificial neural networks for prediction of high pressure vapor-liquid equilibrium, *Australian Journal of Basic and Applied Sciences*, vol.3, no.3, pp.1851-1862, 2009.

[44] H. Shi and W. Li, Evolving artificial neural networks using simulated annealing-based hybrid genetic algorithms, *Journal of Software*, vol.5, no.4, pp.353-360, 2010.

[45] N. Garca-Pedrajas, C. Hervs-Martnez and J. Muoz-Prez, Covnet: A cooperative coevolutionary model for evolving artificial neural networks, *IEEE Transactions on Neural Network*, vol.14, no.3, pp.575-596, 2003.